CrossMark

Poly(phenylmethylsiloxane) functionalized multiwalled carbon nanotube/poly(dimethylsiloxane) nanocomposites with high piezoresistivity, low modulus and high conductivity

Biao Zhang[1] · Buyin Li[1] · Shenglin Jiang[1]

Abstract A high performance of piezoresistive materials can be used to detect the sense of touch. Poly(phenylmethylsiloxane) functionalized multi-walled carbon nanotubes (P-MWCNTs) is introduced into poly(dimethylsiloxane) (PDMS) matrix to obtain P-MWCNTs/PDMS nanocomposites with high performance. The P-MWCNTs with core–shell structure exhibits excellent compatibility in chloroform and homogenous dispersion in PDMS matrix, which is the effective method to dramatically improve the electrical, elastic and piezoresistive properties of nanocomposites. Slightly above the percolation threshold (0.74 vol%) content, the P-MWCNTs/PDMS nanocomposites with 0.75 vol% of P-MWCNTs shows high performance of S of 8.09×10^{-3} KPa^{-1} at finge-sensing regimes (0–100 KPa), low E of 489.50 KPa and high σ of 1.24×10^{-4} S/m. Our work provide a simple, low cost and effective method to prepare high-performance nanocomposites, facilitating the wide applications of piezoresistive materials, especially in the cheap and flexible tactile sensors.

✉ Buyin Li
    libuyin@mail.hust.edu.cn

✉ Shenglin Jiang
    jsl@mail.hust.edu.cn

    Biao Zhang
    95347380@qq.com

[1] School of Optical and Electronic Information, Huazhong University of Science and Technology, No. 1037, Luoyu Road, Wuhan 430074, China

1 Introduction

Due to the inherent advantages of flexibility, light weight and ease of produce, piezoresistive materials have drawn considerable attention during the past decades [1–4]. They have been found significant and various potential applications in flexible tactile sensors of electronic skin, artificial intelligence and wearable health care devices [5–8]. These devices usually require high-performance nanocomposites with properties of high piezoresistive sensitivity (S), low Young's modulus (E) and high electrical conductivity (σ) [9–11]. Moreover, the evaluating of S in the finge-sensing regimes (0–100 KPa) is a key limitation for the practical application [12].

The nanocomposites with metallic particles as conductive fillers shows remarkable S, owing to their high intrinsic electrical conductivity [13]. However, to form a conductive network, the high filler loading could large increase in elastic modulus, resulting in destroying the flexibility of nanocomposites [9, 13]. To maintain the intrinsic flexibility, a number of studies have focused on decreasing the percolation threshold (φ_c) of nanocomposites to improve S [14, 15]. Due to the high aspect ratio (>1000) and high electrical conductivity ($\sigma > 100$ S/cm), multi-walled carbon nanotubes (MWCNTs) are widely used as ideal fillers to prepare the high piezoresistive sensitivity of nanocomposites [16]. However, pristine MWCNTs are not compatible with all solvents, and hence, difficulty arises in obtaining a stable suspension due to chemical inertness. Additionally, they are also very easy to aggregate on account of the Van der Waals force, which lead to poor dispersion especially when they are applied in polymer matrix [17, 18]. Consequently, a large mount of MWCNTs will be needed to form conductive network in polymer matrix, and thus leading to the large increase in φ_c of nanocomposites, resulting in

decrement of *S*. In addition, the high cost and deterioration of flexibility are also not good for the industrial application of nanocomposites [19].

To resolve these problems, one of the most effective ways is the surface functionalization [20–22], which plays a vital role to control the stability of MWCNTs in solvent and the dispersion of MWCNTs in polymer. Although covalently functionalized MWCNTs can introduce oxidative groups to the surface to improve the performance of stability and dispersion, it changes the structure of nanotubes and thus decreases the σ of nanocomposites, largely limiting the wide application of piezoresistive materials [23]. Noncovalently functionalized technique provides a simple and effective method to prepare MWCNTs which maintains the structure and characteristics of MWCNTs [24]. Therefore, introducing noncovalently functionalized MWCNTs into polymer matrix, nanocomposites with high σ is expected to be obtained because of the formation of uniformly and intensively conductive network and the retaining the structure and characteristics of MWCNTs.

In this work, MWCNTs were noncovalent functionalized by poly(phenylmethylsiloxane) (PPMS) as conductive fillers (P-MWCNTs). Poly(dimethyl siloxane) (PDMS) was chosen as the polymer matrix since it had a rather low Young's modulus (<1 MPa), transparency and flexibility for the potential application as tactile sensors [21, 25]. The characterization and nanostructure of P-MWCNTs, the compatibility of P-MWCNTs in chloroform and dispersibility of P-MWCNTs/PDMS nanocomposites, and electrical, elastic and piezoresistive properties of P-MWCNTs/PDMS nanocomposites were systematic examined. To the best of our knowledge, this is the first work describing the effects of P-MWCNTs/PDMS nanocomposites with high piezoresistivity, low Young's modulus and high conductivity. P-MWCNTs/PDMS composites with high performance could potentially be used as piezoresistive materials for cheap and flexible touch sensors.

2 Experimental

2.1 Materials

Multi-walled carbon nanotubes (MWCNTs, diameter 10–20 nm, length 10–30 μm, purity 95 wt%, Hengqiu Graphene Technology (Suzhou) Co. Ltd.) was used as conductive fillers materials. The poly(phenylmethylsiloxane) (PPMS, Molecular weight (M_w) $\approx$ 2500–2700 g/mol) was purchased from Alfa Aesar. Chloroform (>99.5 wt%) was obtained from Sinopharm Chemical Reagent Co., Ltd. The silicone rubber used was poly(dimethylsiloxane) (PDMS, Guiyou new technology (Shanghai) Co. Ltd.). The PDMS was supplied in liquid form which consisted of Part-A and Part-B (Part-A: Base and Part-B: Curing agent).

2.2 Preparation of P-MWCNTs and P-MWCNTs/ PDMS nanocomposites

The preparation process of P-MWCNTs/PDMS nanocomposites was shown in Fig. 1. Firstly, the pristine MWCNTs was noncovalently functionalized by PPMS (P-MWCNTs) to form organic layer on the surfaces of MWCNTs. Secondly, the P-MWCNTs exhibited excellent dispersibility in PDMS matrix, and then the hydrosilation reaction was carried to form P-MWCNTs/PDMS nanocomposites. Details as follow:

The P-MWCNTs was synthesized via a facile one-step noncovalently functionalized method [26]: (1) A mixture containing 1 g of MWCNTs and 2 g of PPMS in 50 milliliter of chloroform was ultrasonicated for 10 min at 25 °C. (2) the suspension were filtrated with Teflon filter (0.3 μm) and washed by chloroform for 3–4 times. (3) The resulting PPMS-functionalized MWCNTs (P-MWCNTs) were then dried under vacuum at 120 °C for 1 h.

The P-MWCNTs/PDMS nanocomposites were prepared by solution casting method: (1) Weighted amount
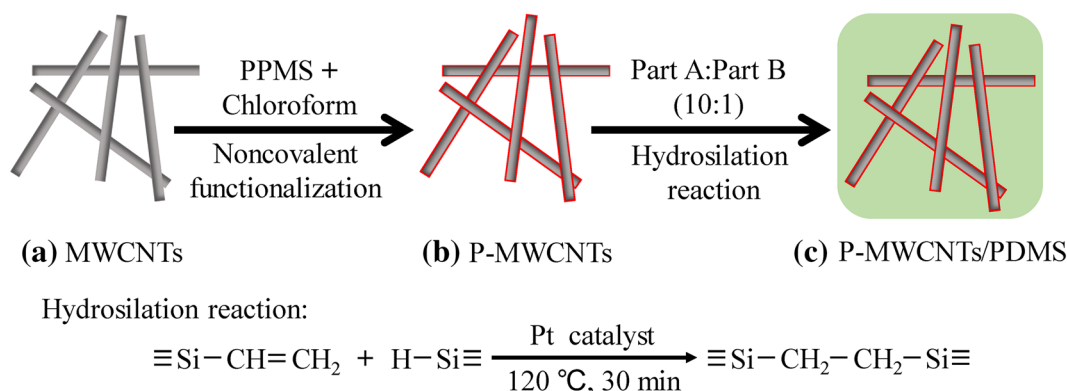

Fig. 1 Schematic illustration of preparation of P-MWCNTs and P-MWCNTs/PDMS nanocomposites

of pristine MWCNTs were dispersed in 50 ml chloroform separately and sonicated in an ultrasonic bath for 10 min achieve uniform dispersion. (2) The P-MWCNTs/chloroform suspension were added into the PDMS (Part-A: Base) and mechanically stirred for 10 min at 80 °C to completely evaporate the chloroform. (3) After the mixture was cooled to room temperature, the PDMS (Part-B: Curing agent) was added in the mixture: cross-link agent ratio of 10:1 (Part-A: Part-A) in mass and the mixture was again stirred for 10 min at room temperature. (4) After degassing under vacuum for 10 min, those viscous mixtures were molded onto the flexible polyamide (PI) substrates on which were painted with parallel silver paste as electrodes, and then cured at 120 °C for 30 min to form a thin film with a size of $20 \times 10 \times 4$ mm.

2.3 Characterization

The characteristics and nanostructure of P-MWCNTs were examined by X-ray diffraction (XRD, PANalytical B.V., X'Pert PRO), Fourier transform infrared (FTIR, Bruker, VERTEX-70), Thermogravimetric analysis (TGA, NETZSCH, STA 449), Transmission electron microscopy (TEM, FEI, Tecnai-G2 20). The surface morphology of P-MWCNTs in the PDMS matrix was analyzed using field emission scanning electron microscope (FE-SEM, FEI, Sirion-200). The electrical properties of the composites were measured using an multimeter agilent 34401a by four-wire (Europe, Kelvin) measurement [27]. The electrical conductivity (σ) was then computed use the equation:

$$\sigma = \frac{1}{\rho} = \frac{L}{R \times A} \tag{1}$$

where σ is electrical conductivity (S/m), ρ is resistivity (Ω mm), A is cross-sectional area (mm^2) and L is length (mm). Elastic and piezoresistive properties were performed to determine uniaxial compression utilizing an electronic universal testing machine (MTS Exceed 40.SANS.China) with a constant rate of speed of 0.2 mm/min.

3 Results and discussion

3.1 Characterization and nanostructure of P-MWCNTs

3.1.1 XRD analysis of P-MWCNTs

Figure 2 shows the characterization of pristine MWCNTs, the P-MWCNTs, and pure PPMS which are investigated by the X-ray diffraction (XRD). As shown in Fig. 2a, the PPMS shows two broad peaks centered at about $2\theta = 9.5°$

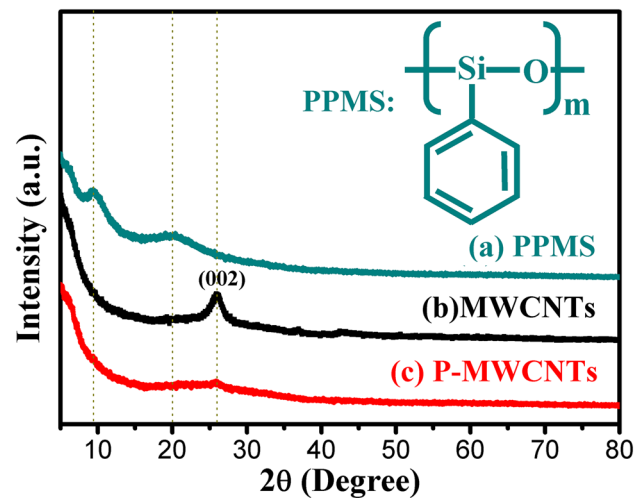**Fig. 2** XRD of (*a*) PPMS, (*b*) pristine MWCNTs, and (*c*) P-MWC-NTs

and 21°, which means it is a typical amorphous structure. For pristine MWCNTs (see Fig. 2b), a peak at $2\theta = 26.6°$ is clearly observed, which is ascribed to the ordered crystallized structure of MWCNTs [28]. After the MWCNTs is noncovalently functionalized by the PPMS (see Fig. 2c), the characteristic peak of P-MWCNTs does not change but the shape of peaks weakened. This indicates that no new phase transformation of P-MWCNTs occurs during the noncovalently functionalized preparation step, and that the surface of P-MWCNTs is stacked by PPMS well [29].

3.1.2 FT-IR analysis of P-MWCNTs

FT-IR results of pristine MWCNTs, P-MWCNTs, and pure PPMS are shown to prove the PPMS are stacked on the surface of MWCNTs, which are displayed in Fig. 3. As can be seen, almost no absorption peak is observed in the curve of pristine MWCNTs (Fig. 3a). Obviously, both the P-MWCNTs (Fig. 3b) and pure PPMS (Fig. 3c) show C-H stretching vibration peaks at 3069 cm^{-1}, which is characteristic of the phenyl group [21]. Meanwhile, three absorption peaks at about 841, 731, and 698 cm^{-1}, which are due to phenyl-ring substitution bands of pure PPMS [30]. It proves that new noncovalent bond of phenyl-ring is formed on the surface of P-MWCNTs. In addition, samples of P-MWCNTs and pure PPMS both show both peaks at 1260 and 1125 cm^{-1} are appeared in both curves of P-MWCNTs and PPMS, which are ascribed to the Si–O stretching from PPMS [31]. These results indicate that the surfaces of the P-MWCNTs have been noncovalently functionalized by PPMS.
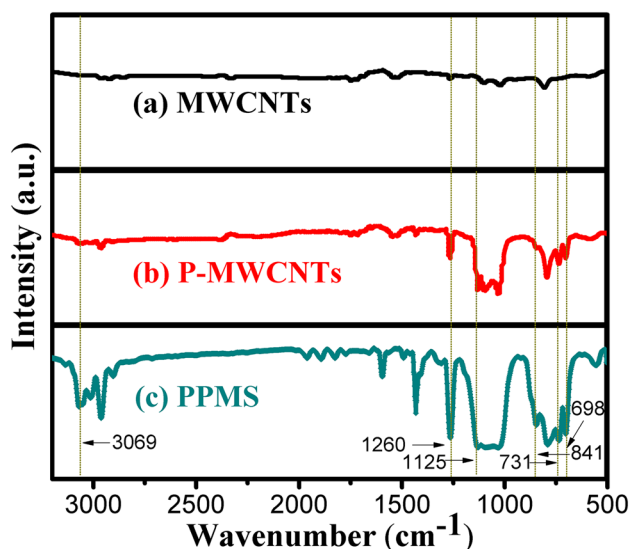
Fig. 3 FT-IR of (*a*) pristine MWCNTs, (*b*) P-MWCNTs, and (*c*) PPMS

3.1.3 TEM analysis of P-MWCNTs

The nanostructure of pristine MWCNTs, and P-MWCNTs are exhibited in TEM images (Fig. 4). Due to the high aspect ratio of MWCNTs, the pristine MWCNTs tend to

aggregate and entangle instigated by high Vander Waals force attractions. As can be seen from Fig. 4a, b, the pristine MWCNTs show severely intertwined to form coils due to the treatment of sonicate, while the P-MWCNTs exhibit further improved dispersibility without obvious agglomerates and coils due to modifier of PPMS. Figure 4c, d orderly present the images of high-resolution TEM of pristine MWCNTs, and P-MWCNTs. The pristine MWCNTs exhibit clear crystal striations and smooth sidewalls of the nanotubes (see Fig. 4c). By contrast, continuous polymer layers with thickness of 2–3 nm are stacked on the sidewalls of the nanotube in the sample of P-MWCNTs, which is shown in Fig. 4d. These results indicate that the noncovalent functionalization occurs along the side-walls and the PPMS is stacked on the surfaces of MWCNTs.

3.1.4 TG analysis of P-MWCNTs

To confirm content of PPMS layer on the surfaces of pristine MWCNTs, the TGA curves of pristine MWCNTs, P-MWCNTs, and pure PPMS are investigated, which are shown in Fig. 5. As can be seen that: (i) there is no visible weight loss below 250 °C of the pure PPMS, which is attributed to the high boiling point of polymer; (ii) the weight loss of the samples show the sequence of MWCNTs < P-MWCNTs < PPMS under 650 °C; (iii) the
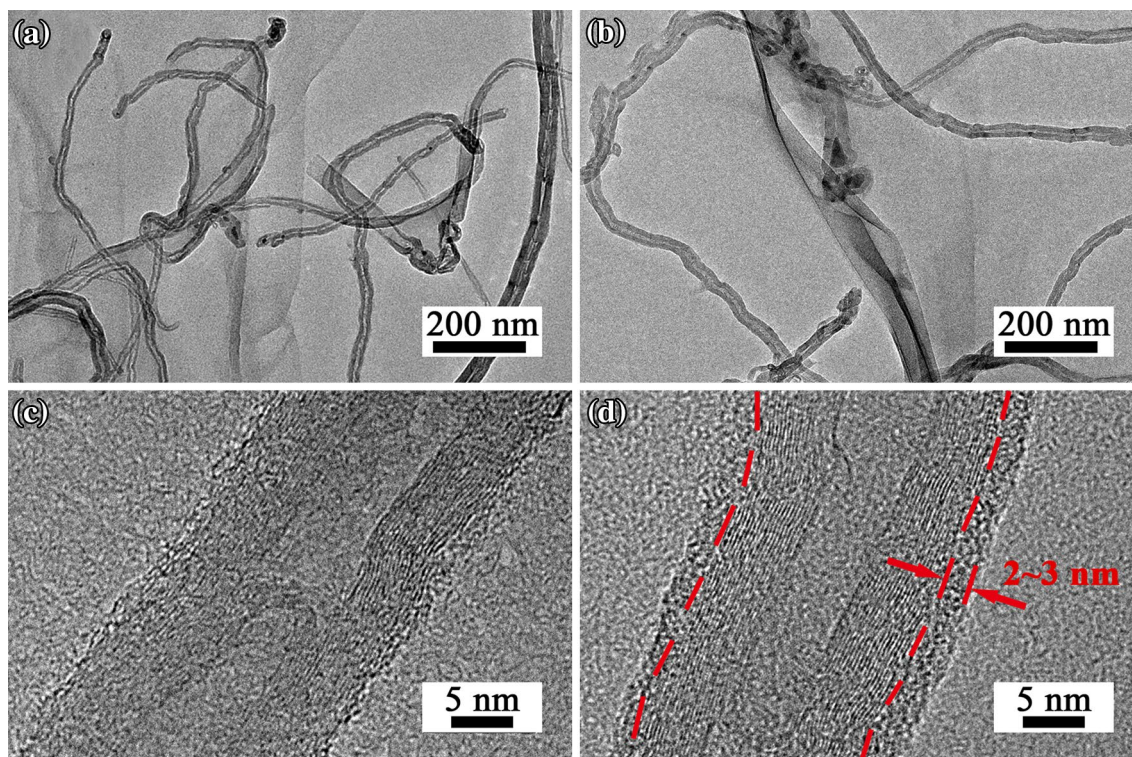

Fig. 4 TEM images of pristine MWCNTs with **a** low magnification and **c** high magnification; P-MWCNTs with **b** low magnification and **d** high magnification
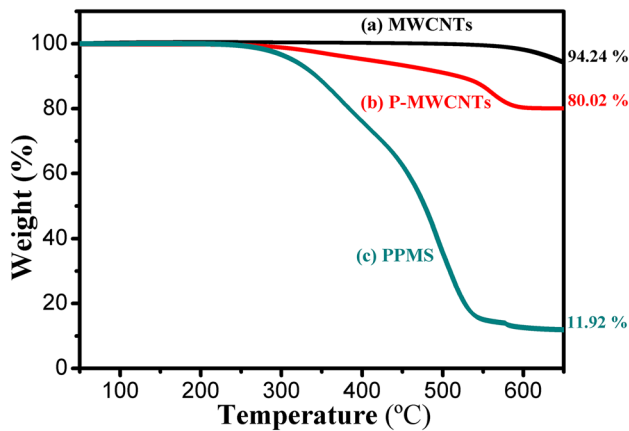
Fig. 5 TGA curves of (*a*) pristine MWCNTs, (*b*) P-MWCNTs, and (*c*) PPMS

P-MWCNTs and PPMS exhibit a dramatic weight loss from about 300 to 600 °C, which is resulted from the thermal decomposition of organic molecules. The weight loss of P-MWCNTs (19.98%) is attributed to both loss of MWC-NTs and PPMS because the weight loss of MWCNTs and pure PPMS are almost 5.76 and 88.08% at 650 °C, respectively. Based on the result of TGA, the weight fraction of PPMS that stacked on the surface of MWCNTs could be calculated, which is about 17.27%.

3.2 Compatibility and dispersibility of P-MWCNTs and P-MWCNTs/PDMS nanocomposites

3.2.1 Compatibility of P-MWCNTs in chloroform

Figure 6 shows the photographs of solution stability of the pristine MWCNTs, and P-MWCNTs suspension after being stood for 1 min, 1 h, 1 day, and 1 week. All of the samples are mixed with chloroform and treated by sonication for 10 min at 25 °C. It is clear that pristine MWCNTs quickly settled to bottom of the bottle, which is due to higher density of MWCNTs than that of chloroform and the incompatibility between MWCNTs and chloroform. The MWCNTs indeed exhibit better stability after being noncovalently functionalized by PPMS. Compared with the MWCNTs, the P-MWCNTs suspension still show dark color even after the suspension stand for 1 week. These results indicate that the PPMS indeed is an effective modifier for improving the dispersibility of MWCNTs.

3.2.2 Dispersibility of P-MWCNTs/PDMS nanocomposites

The cross-section SEM images of the P-MWCNTs/PDMS nanocomposites are shown in Fig. 7. We can observe that the fractured surface of neat PDMS (0.00 vol%) is clear and

smooth, as seen in Fig. 7a. The fractured surface of all the nanocomposites with 0.50, 1.00, 1.50 vol% of P-MWCNTs exhibits many ripples and corrugations, representing the presence of P-MWCNTs, as shown in Fig. 7b–d. Due to the good dispersibility of P-MWCNTs in PDMS matrix, very few of nanotubes and negligible agglomerations can be seen in the cross sections of the nanocomposites when the content of P-MWCNTs is 0.50 vol%. The conductive network of P-MWCNTs connect with one another is gradually formed by the increase in the content of P-MWCNTs to 1.00 vol%. Most of the P-MWCNTs are coated by the PDMS matrix and homogeneously dispersed. Since the TEM image (Fig. 4d) shows that the thickness of the PPMS layer on the surface of MWCNTs is about 2–3 nm, the nearest distance between adjacent MWCNTs is exceed 4 nm, which plays an important role in obtaining better dispersion by reducing the Vander walls force between MWCNTs [32]. In addition, slight agglomerations of the P-MWCNTs can be observed in the PDMS matrix when the content was up to 1.50 vol%, which implys that the nanocomposites with 1.50 vol% P-MWCNTs has already exceeded the percolation threshold.

The uniform dispersion of the P-MWCNTs in the PDMS matrix could be further investigated by the XRD patterns shown in Fig. 8. For the P-MWCNTs, the characteristic peak corresponds to the pristine MWCNTs ($2\theta = 26.6°$, see Fig. 2). After the P-MWCNTs are incorporated in to the PDMS matrix, the characteristic peak of the neat PDMS (12.4°) does not change and no P-MWCNTs peak is observed, which suggests that the PDMS chains have efficiently mixed with P-MWCNTs. It should be noted that the intensity of nanocomposites decreases with increasing added content of P-MWCNTs, which implys that P-MWC-NTs successfully disperse in PDMS matrix well [33].

3.3 Characterization of P-MWCNTs/PDMS nanocomposites

3.3.1 Electrical properties of P-MWCNTs/PDMS nanocomposites

The electrical percolation effect is one of the most important signals of forming the conductive network. Hence, the influence of pristine MWCNTs, and P-MWCNTs on the electrical percolation behavior of nanocomposites is represented in Fig. 9, which show the variation of electrical conductivities with different fillers content. The incorporation of the P-MWCNTs from 0.50 to 0.75 vol% increased the electrical conductivity almost five orders of magnitude, from 5.23×10^{-9} S/m to 1.24×10^{-4} S/m (see Table 1). This observation can be explained in term of percolation theory [34]. According to percolation theory:

$$\sigma = \sigma_0 (\varphi - \varphi_c)^t \tag{2}$$
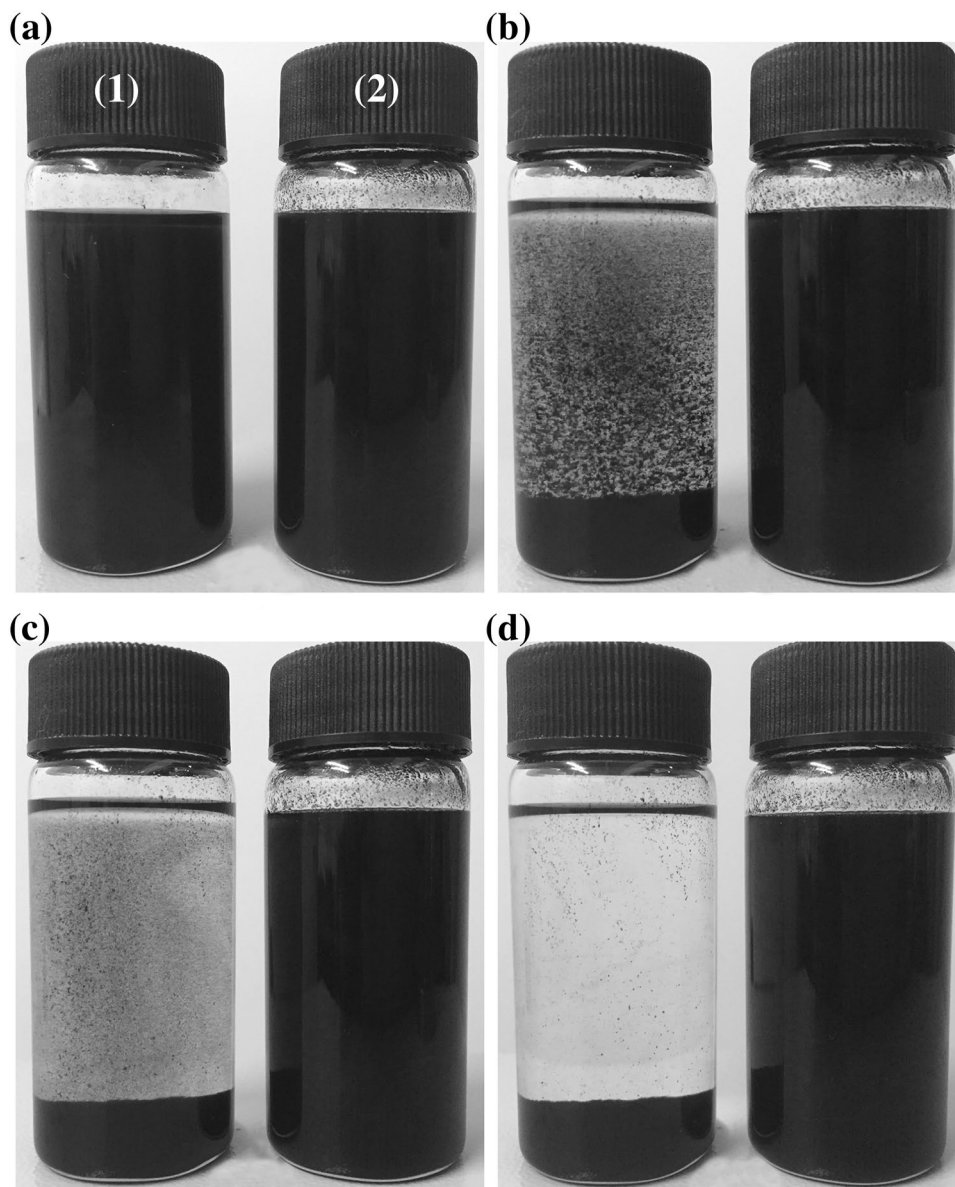
where σ is the electrical conductivity, σ_0 is the proportionality constant related to the intrinsic conductivity of the fillers, '*t*' is the critical exponent, φ is the volume fraction of MWCNTs, and φ_c is the percolation threshold, which represents a best fits to the experimentally measured conductivity date (inset in Fig. 9; Table 1). In case of the P-MWC-NTs/PDMS nanocomposites, the percolation threshold appears 0.74 vol%, while it is 9.10 vol% for MWCNTs/PDMS nanocomposites. Such low percolation value for P-MWCNTs is due to PPMS can not only decrease the fillers agglomeration itself but also improve dispersion of fillers in polymer matrix. It is certainly that P-MWCNTs can form the uniformally and intensively conductive network in PDMS matrix. Thus, contacts of internal conductive network of nanocomposites are effectively enhanced and the percolation threshold is dramatically decreased.

3.3.2 Elastic properties of P-MWCNTs/PDMS nanocomposites

The elastic properties of these nanocomposites for different volume percentage of P-MWCNTs are evaluated via monotonic uniaxial compressive tests. The stress–strain curves [whose slopes represent the Young's modulus (*E*)] of the nanocomposites for different volume percentage of P-MWCNTs presented in Fig. 10. As the P-MWCNTs loading is increased, the Young's modulus increase. The results are compared with that of neat PDMS matrix.
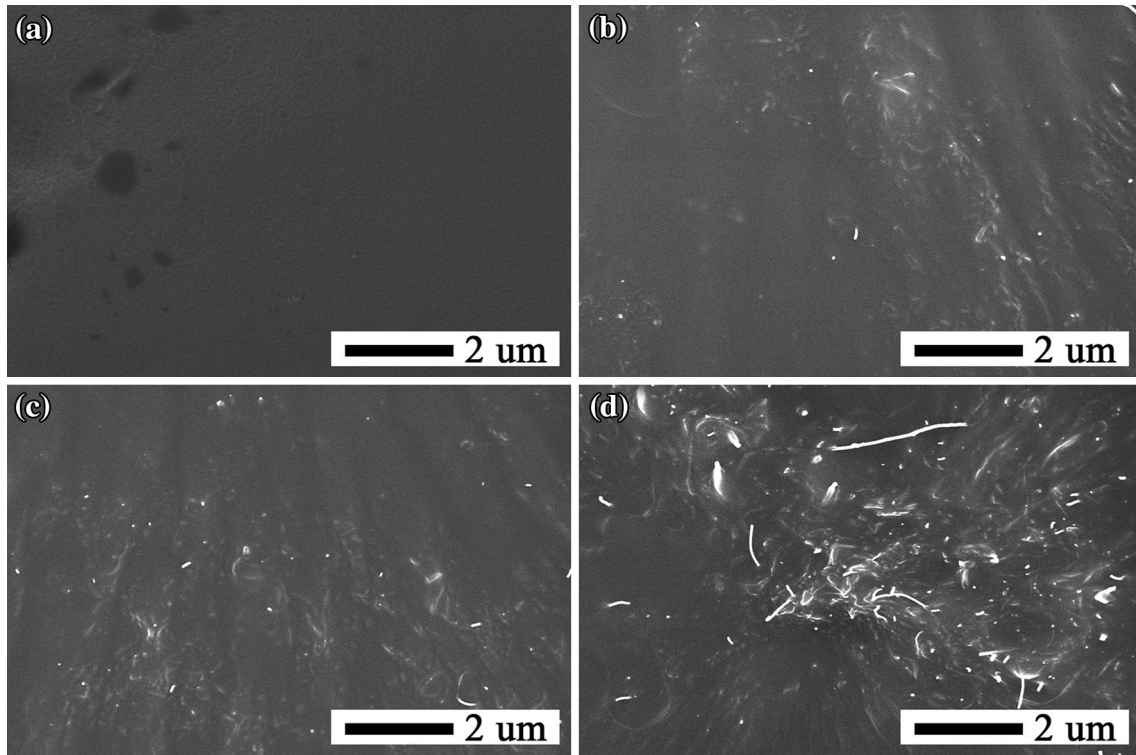
Fig. 7 The cross sectional SEM images of the nanocomposites with **a** 0 vol%, **b** 0.5 vol%, **c** 1.0 vol%, and **d** 1.5 vol% P-MWCNTs
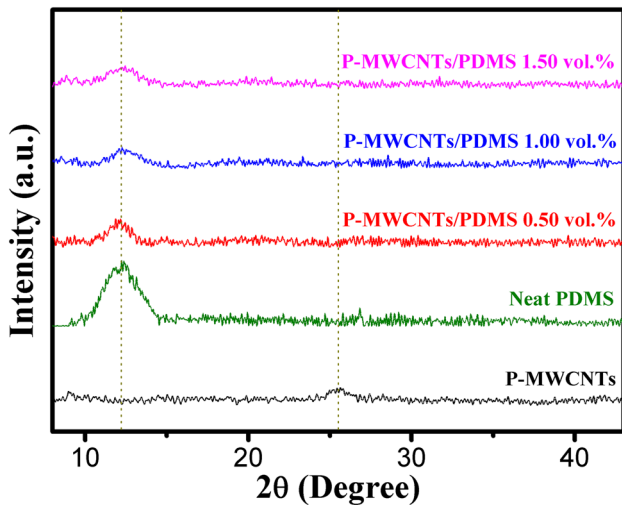

Fig. 8 XRD patterns of P-MWCNTs and the P-MWCNTs/PDMS nanocomposites

Fig. 9 The electrical properties of MWCNTs/PDMS and P-MWC-NTs/PDMS nanocomposites. The *inset* shows the best fit of log (σ) versus log ($\varphi - \varphi_c$)

Figure 11 shows Young's modulus which increases almost linearly up to the 0.75 vol%. Beyond 1.00 vol% of P-MWCNTs there is not much improvement in Young's modulus. The error in the Young's modulus value at the 0.75 vol% of P-MWCNTs is very high in the data because of the experimental e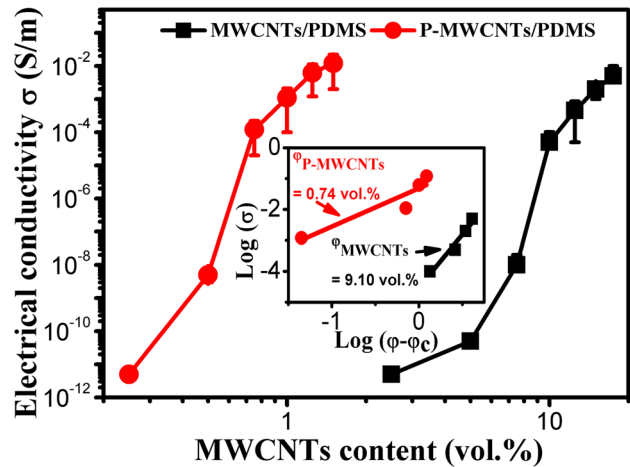rror induced probably by the uneven distribution of P-MWCNTs and non-uniformity of the samples thickness. Young's modulus is summarized in Table 1. With the addition of 0.25, 0.75, and 1.00 vol% of P-MWCNTs in PDMS matrix, the Young's modulus is observed to be increased by 4.66, 32.39, and 39.45%, respectively.

Table 1 Electrical, mechanical and electromechanical properties of P-MWCNTs/PDMS nanocomposites as a function of P-MWCNTs content

Properties	Vol% of P-MWCNTs in PDMS matrix						
	0.00	0.25	0.50	0.75	1.00	1.25	1.50
Electrical conductivity (S/m)	–	5.46×10^{-12}	5.23×10^{-9}	1.24×10^{-4}	1.15×10^{-3}	6.22×10^{-3}	1.27×10^{-2}
Young's modulus (KPa)	369.74	386.98	438.23	489.50	515.62	518.09	522.18
Piezoresistive sensitivity (KPa^{-1})	–	1.44×10^{-3}	1.71×10^{-3}	8.09×10^{-3}	4.57×10^{-3}	3.31×10^{-3}	2.74×10^{-3}
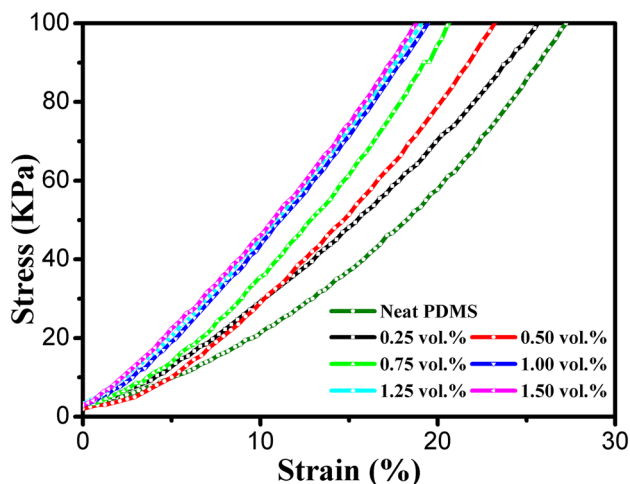
Fig. 10 Stress–Strain behavior of P-MWCNTs/PDMS nanocomposites as a function of P-MWCNTs content
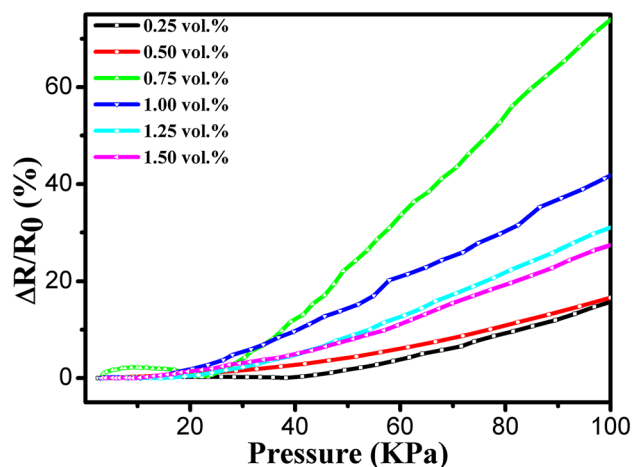
Fig. 12 Piezoresistive behavior of P-MWCNTs/PDMS nanocomposites as a function of P-MWCNTs content
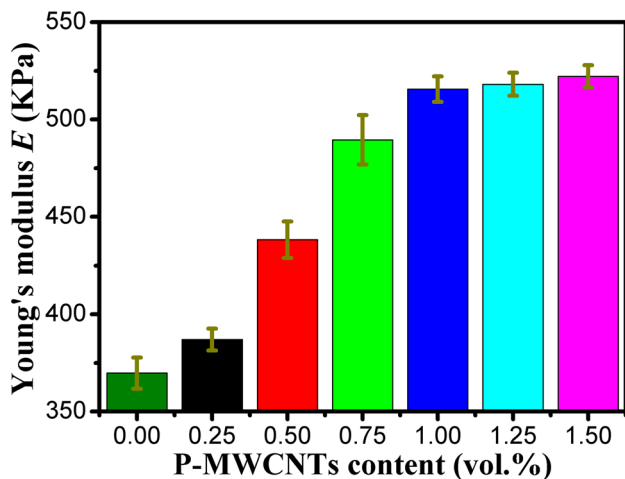
Fig. 11 Young's modulus of P-MWCNTs/PDMS nanocomposites as a function of P-MWCNTs content

3.3.3 Piezoresistive properties of P-MWCNTs/PDMS nanocomposites

Figure 12 shows the response of the P-MWCNTs/PDMS nanocomposite in terms of percentage change in relative resistance at various volume percentage of P-MWCNTs.

Change in relative resistance increases with increasing applied pressure. They all present a remarkable positive pressure-sensitive effect (PPC). Even though there is not much change in the relative resistance for the 0.25 and 0.50% volume percentage P-MWCNTs, the relative resistance increases with applied pressure as the P-MWCNTs loading increases. This trend continued up to the content of 0.75 vol% and then a decreasing trend in the change in relative resistance is observed up to 1.50 vol%. Change in relative resistance of P-MWCNTs/PDMS nanocomposites when applied pressure occurs due to deformation induce a variation of the conductive network and then change the tunneling distance of neighboring P-MWCNTs, result in the change of tunneling resistance of P-MWCNTs/PDMS nanocomposites. As the P-MWCNTs content increases, conductive paths are formed by the network of P-MWCNTs. At the percolation threshold, this path is just formed and electrical conductivity increases significantly. If the nanocomposite is pressured at this content, breakage of conductive path occurs and a drastic change in relative resistance can be observed. Above this threshold, several alternative conductive paths are available which results in minor change in relative resistance leading to decreased piezoresistive sensitivity.

Here, the piezoresistive sensitivity (S) can be described [35]:

$$S = \frac{\delta(\Delta R/R_0)}{\delta P} \qquad (3)$$

where R is the resistance under pressure, R_0 is the original resistance, P is the applied pressure, S also reflects the sensitive degree of change in the relative resistance versus pressure. The S of these nanocomposites as a function of P-MWCNTs content is calculated, given in Fig. 13 and Table 1. The piezoresistive sensitivity of the 0.25 and 0.50 vol% of P-MWCNTs/PDMS nanocomposites is low with a S of 1.44×10^{-3} and 1.71×10^{-3} KPa^{-1}. At slightly above percolation threshold of 0.75 vol%, a good piezoresistive sensitivity is obtained with a S of 8.09×10^{-3} KPa^{-1}. Above this loading fraction, the S reduces with increase in P-MWCNTs fraction and saturation is obtained at 1.25 vol% of P-MWCNTs.

4 Conclusions

The P-MWCNTs was obtained by a noncovalent functionalized PPMS on the surface of pristine MWCNTs, which was introduced to the PDMS matrix with various loadings. Continuous PPMS shell layers with thickness of 2–3 nm were stacked to the sidewalls of the MWCNTs, and the P-MWCNTs with core–shell structure exhibited outstanding compatibility in chloroform and homogeneously dispersibility in PDMS matrix. To meet the practical demands, high performance of P-MWCNTs/PDMS nanocomposites should be simultaneously achieved slightly above the percolation threshold (0.74 vol%) content. The nanocomposites with 0.75 vol% of P-MWCNTs shows high S of 8.09×10^{-3} KPa^{-1} at finge-sensing regimes (0–100 KPa),
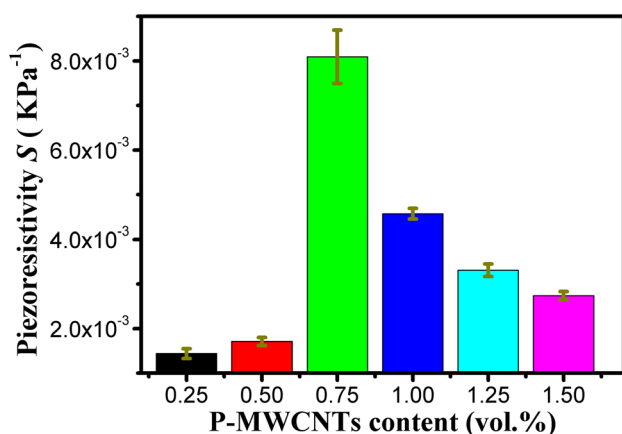
low E of 489.50 KPa and high σ of 1.24×10^{-4} S/m. Thus, the P-MWCNTs/PDMS nanocomposites with high performance have potential applications as flexible touch sensors.

References

1. D.J. Lipomi, M. Vosgueritchian, B. Tee et al., Nat. Nanotechnol. **6**, 788–792 (2011)
2. J. Park, Y. Lee, J. Hong et al, ACS. Nano **8**, 12020–12029 (2014)
3. L. Pan, A. Chortos, G. Yu et al, Nat. Commun. **5**, 1–8 (2014)
4. Y. Yang, B. Zhu, D. Yin et al., Nano. Energy **17**, 1–9 (2015)
5. M. Kaltenbrunner, T. Sekitani, J. Reeder et al., Nature **499**, 458–463 (2013)
6. G.A. Salvatore, N. Münzenrieder, T. Kinkeldei et al, Nat. Commun. **5**, 1–8 (2014)
7. K. Takei, W. Honda, S. Harada et al, Adv. Healthc. Mater. **4**, 487–500 (2015)
8. Y. Zang, F. Zhang, C. Di et al, Mater. Horiz. **2**, 140–156 (2015)
9. H. Zhao, J. Bai, ACS Appl. Mater. Inter. **7**, 9652–9659 (2015)
10. S. Jung, J.H. Kim, J. Kim et al., Adv. Mater. **26**, 1–6 (2014)
11. J. Zhao, G. Wang, R. Yang et al., ACS Nano **9**, 1622–1629 (2015)
12. S.C.B. Mannsfeld, B.C.-K. Tee, R.M. Stoltenberg et al., Nat. Mater. **9**, 859–864 (2010)
13. G. Canavese, S. Stassi, C. Fallauto et al, Sens. Actuators. A **208**, 1–9 (2014)
14. N. Hu, Y. Karube, M. Arai et al., Carbon **48**, 680–687 (2010)
15. H. Deng, L. Lin, M. Ji et al., Prog. Polym. Sci. **39**, 627–655 (2014)
16. L. Hu, D.S. Hecht, G. Grüner et al., Chem. Rev. **110**, 5790–5844 (2010)
17. C. Cattin, P. Hubert, ACS Appl. Mater. Inter. **6**, 1804–1811 (2014)
18. L. Vast, Z. Mekhalif, A. Fonseca et al., Compos. Sci. Technol. **67**, 880–889 (2007)
19. S. Makireddy, S. Shivaprasad, G. Kosuri et al., Compos. Sci. Technol. **118**, 101–107 (2015)
20. M.J. Jiang, Z.M. Dang, S.H. Yao et al., Chem. Phys. Lett. **457**, 352–356 (2008)
21. T.P. Chua, M. Mariatti, A. Azizan et al., Compos. Sci. Technol. **70**, 671–677 (2010)
22. N. Wang, Z. Y. Wang Yu et al., Compos. Part A **78**, 341–349 (2015)
23. S.W. Kim, T. Kim, Y.S. Kim et al., Carbon **50**, 3–33 (2012)
24. P.C. Ma, N.A. Siddiqui, G. Marom et al., Compos. Part A **41**, 1345–1367 (2010)
25. Y. Qin, M.R. Howladera, M.J. Deen et al, Sens. Actuators. B **202**, 758–778 (2014)
26. Z. Wang, X. Ye, Nanotechnology **24**, 265704(10pp) (2013)
27. P. Dharap, Z. Li, S. Nagarajaiah et al., Nanotechnology **15**, 379–382 (2004)
28. S. Shang, L. Gan, M.C. Yuen et al., Compos. Part A **66**, 135–141 (2014)

Fig. 13 Piezoresistive sensitivity of P-MWCNTs/PDMS nanocomposites as a function of P-MWCNTs content

29. F. Wu, J. Chen, L. Li et al., J. Phys. Chem. C **115**, 24411–24417 (2011)
30. L. Wei, Y. Zhang, Chem. Phys. Lett. **446**, 142–144 (2007)
31. T.P. Chua, M. Mariatti, A. Azizan et al, J. Alloy. Compd. **480**, 534–536 (2009)
32. H. Luo, Z. Wu, C. Chen et al., Compos. Part A **86**, 57–65 (2016)
33. L.T. Wang, Q. Chen, R.Y. Hong et al, J. Mater. Sci. Mater. Electron. **26**, 8667–8675 (2015)
34. S.G. Prolongo, M.R. Gude, A. Ureña, Compos. Sci. Technol **71**, 765–771 (2011)
35. B. Zhu, Z. Niu, H. Wang et al., Small **10**, 3625–3631 (2014)